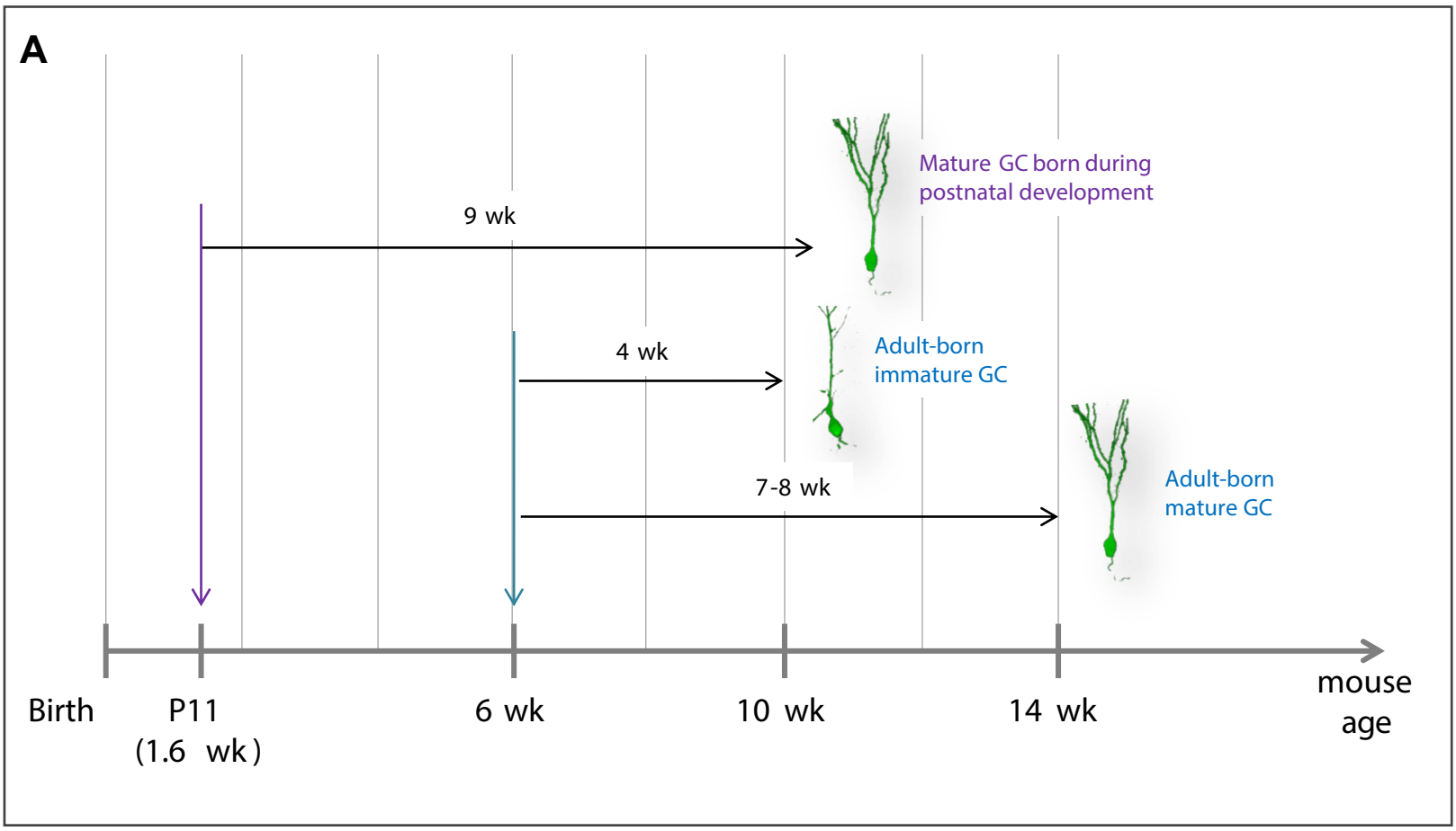
A
9 wk
4 wk
7-8 wk
Mature GC born during
postnatal development
Adult-born
immature GC
Adult-born
mature GC
Birth
P11
(1.6 wk)
6 wk
10 wk
14 wk
mouse
age

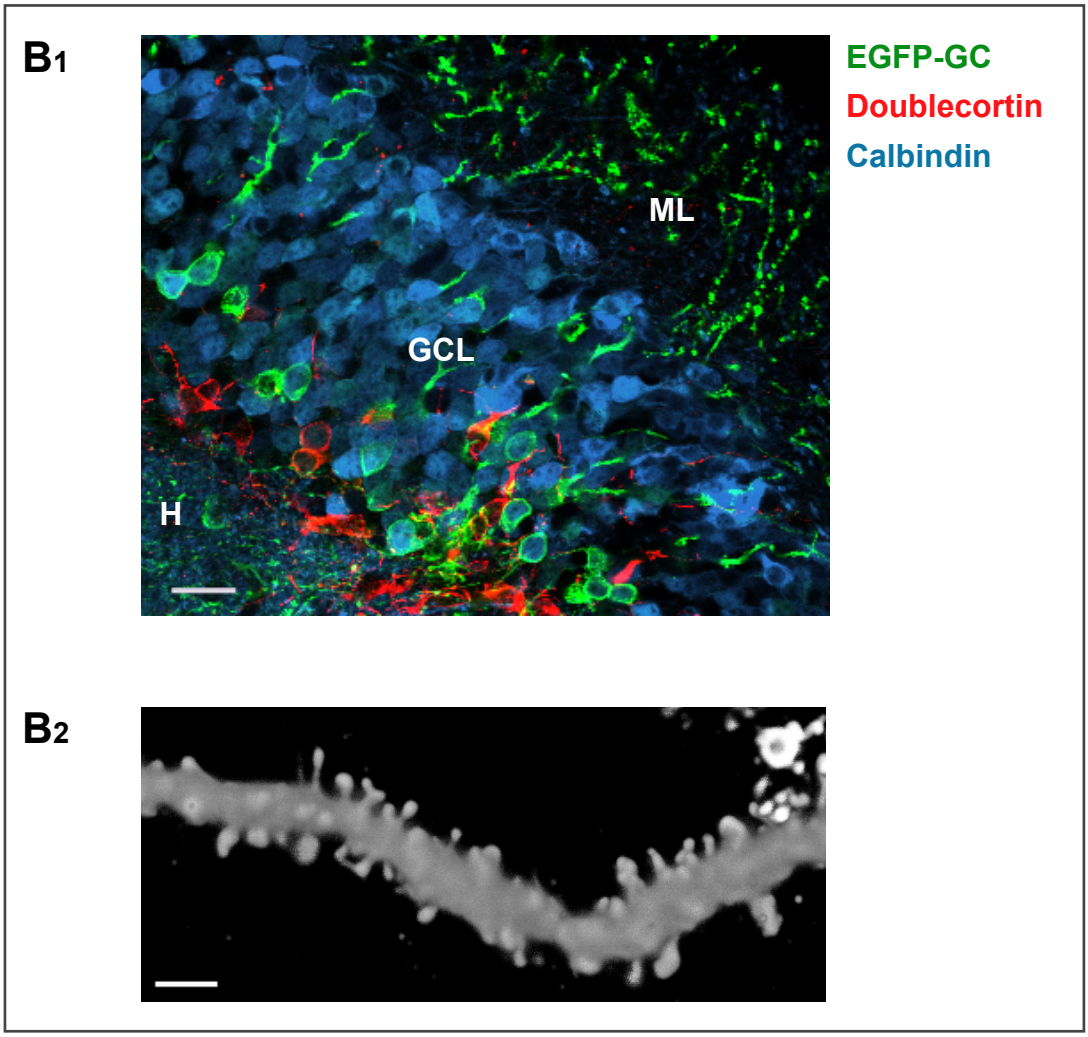
B1
EGFP-GC
Doublecortin
Calbindin
ML
GCL
H
B2

Figure S1

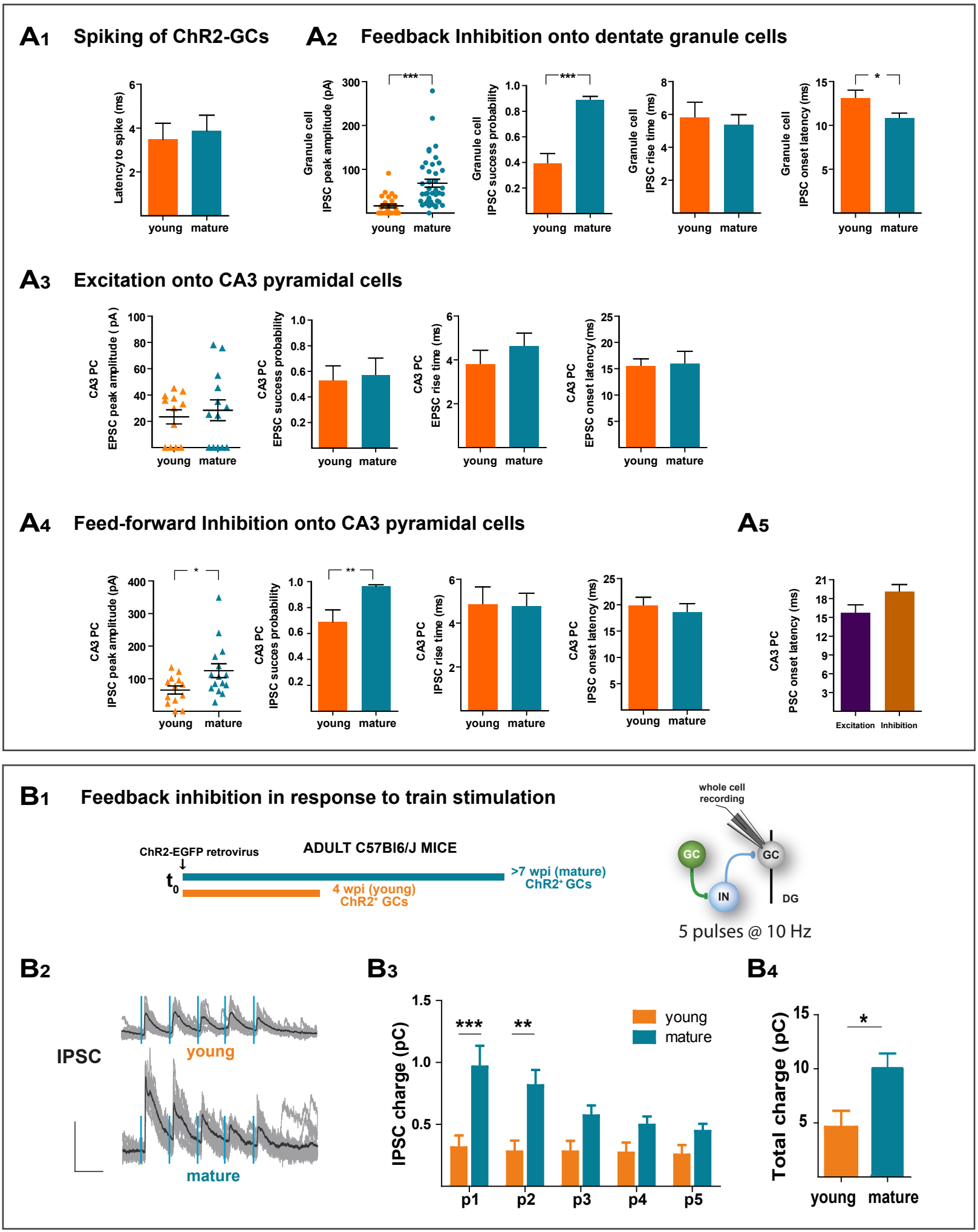
A1
Spiking of ChR2-GCs
Latency to spike (ms)
young
mature
A2
Feedback Inhibition onto dentate granule cells
Granule cell
IPSC peak amplitude (pA)
IPSC success probability
IPSC rise time (ms)
IPSC onset latency (ms)
***
*
A3
Excitation onto CA3 pyramidal cells
CA3 PC
EPSC peak amplitude (pA)
EPSC success probability
EPSC rise time (ms)
EPSC onset latency (ms)
A4
Feed-forward Inhibition onto CA3 pyramidal cells
IPSC peak amplitude (pA)
IPSC succes probability
IPSC rise time (ms)
IPSC onset latency (ms)
**
A5
PSC onset latency (ms)
Excitation
Inhibition
B1
Feedback inhibition in response to train stimulation
ChR2-EGFP retrovirus
ADULT C57Bl6/J MICE
t0
>7 wpi (mature)
ChR2+ GCs
4 wpi (young)
ChR2+ GCs
whole cell
recording
GC
IN
DG
5 pulses @ 10 Hz
B2
IPSC
young
mature
B3
IPSC charge (pC)
young
mature
p1
p2
p3
p4
p5
B4
Total charge (pC)

Figure S2

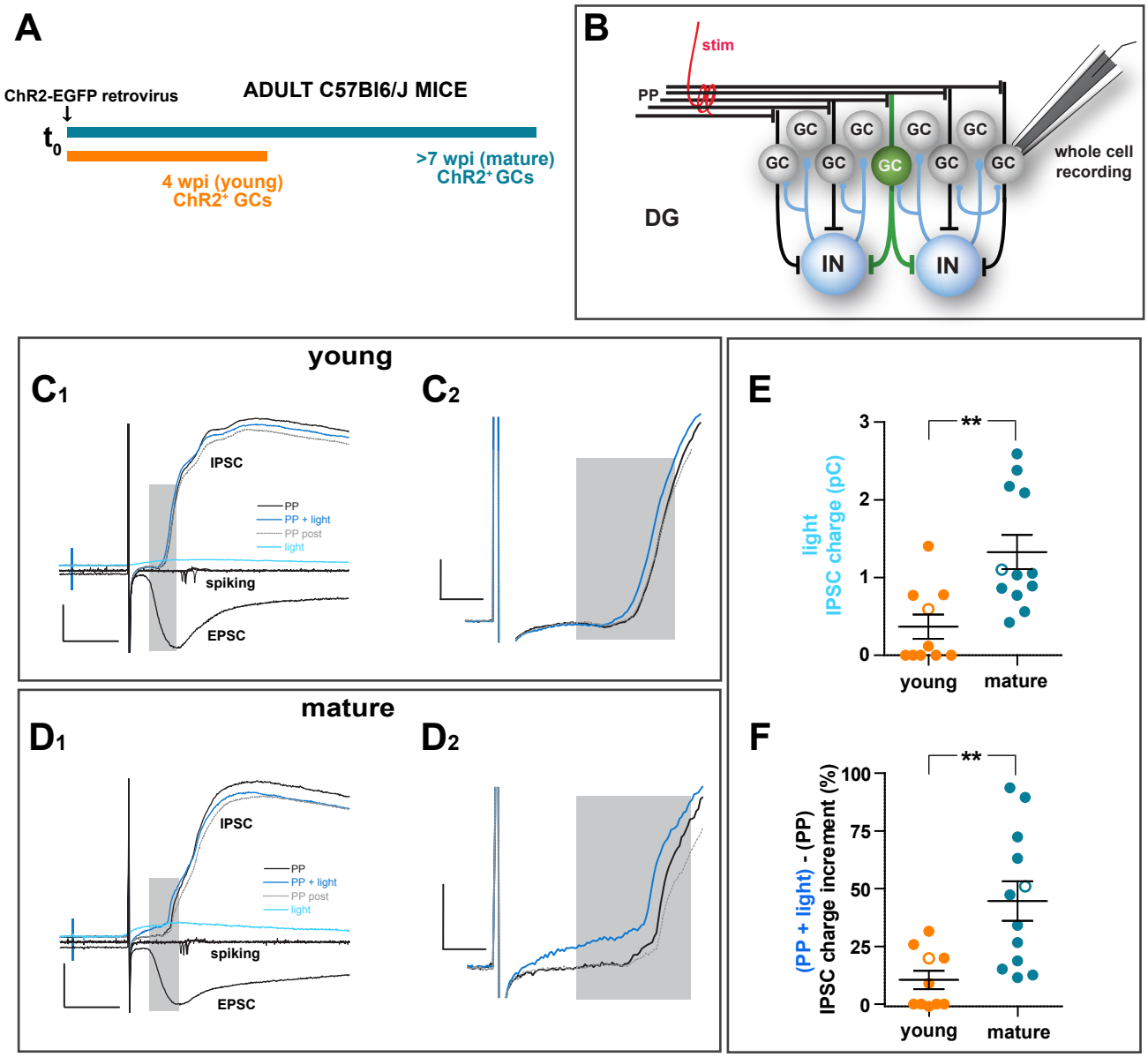
A
ChR2-EGFP retrovirus
ADULT C57Bl6/J MICE
t0
4 wpi (young)
ChR2+ GCs
>7 wpi (mature)
ChR2+ GCs
B
stim
PP
GC
whole cell
recording
DG
IN
young
C1
C2
IPSC
PP
PP + light
PP post
light
spiking
EPSC
mature
D1
D2
E
light
IPSC charge (pC)
young
mature
F
(PP + light) - (PP)
IPSC charge increment (%)

Figure S3

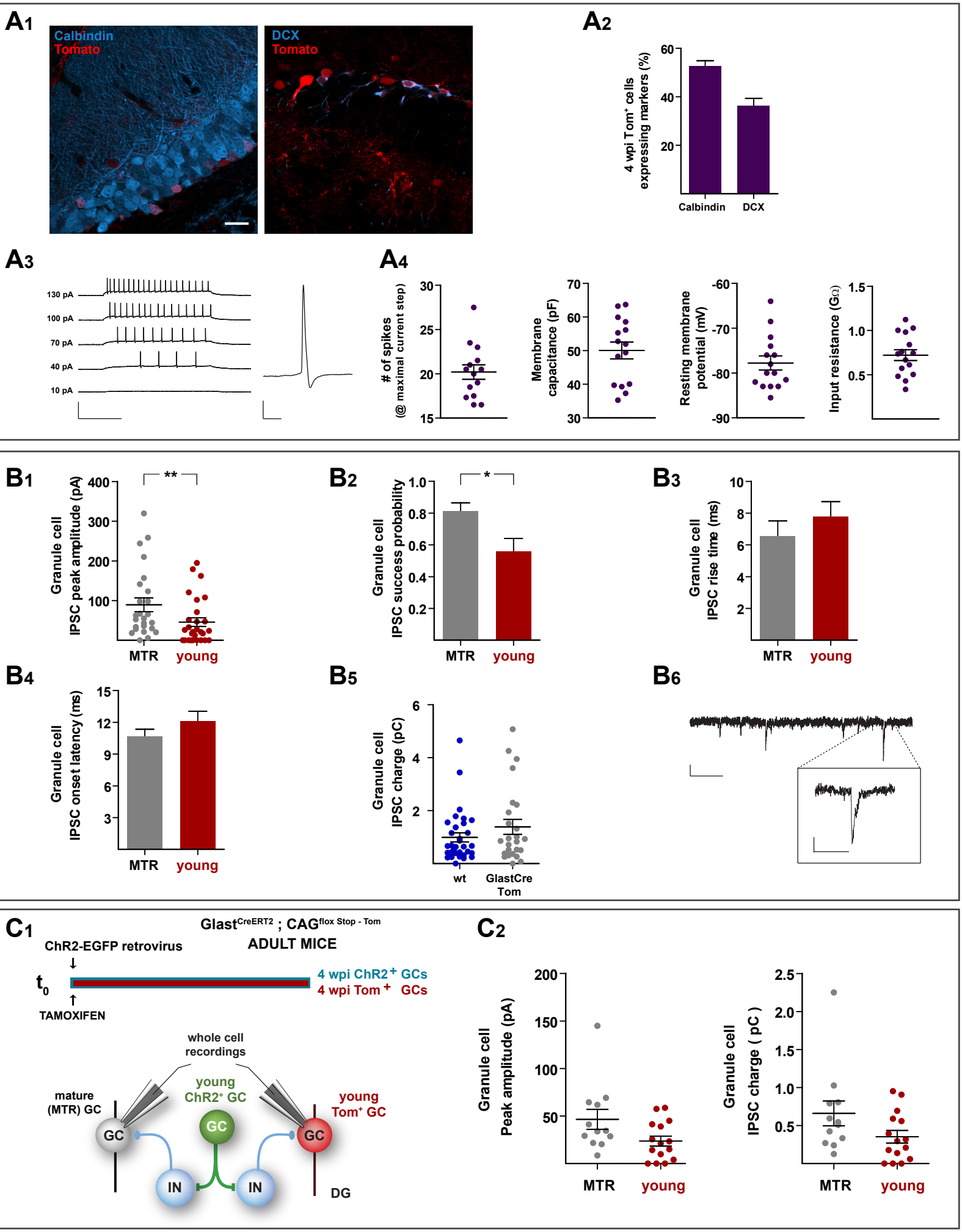
A1
Calbindin
Tomato
DCX
Tomato
A2
4 wpi Tom+ cells expressing markers (%)
60
40
20
Calbindin
DCX
A3
130 pA
100 pA
70 pA
40 pA
10 pA
A4
# of spikes (@ maximal current step)
30
25
20
15
Membrane capacitance (pF)
70
60
50
40
30
Resting membrane potential (mV)
-60
-70
-80
-90
Input resistance (GΩ)
1.5
1.0
0.5
B1
Granule cell IPSC peak amplitude (pA)
400
300
200
100
**
MTR
young
B2
Granule cell IPSC success probability
1.0
0.8
0.6
0.4
0.2
*
MTR
young
B3
Granule cell IPSC rise time (ms)
10
8
6
4
2
MTR
young
B4
Granule cell IPSC onset latency (ms)
15
12
9
6
3
MTR
young
B5
Granule cell IPSC charge (pC)
6
4
2
wt
GlastCre Tom
B6
C1
Glast CreERT2 ; CAG flox Stop - Tom
ADULT MICE
ChR2-EGFP retrovirus
t0
TAMOXIFEN
4 wpi ChR2+ GCs
4 wpi Tom + GCs
whole cell recordings
mature (MTR) GC
young ChR2+ GC
young Tom+ GC
GC
GC
GC
IN
IN
DG
C2
Granule cell Peak amplitude (pA)
200
150
100
50
MTR
young
Granule cell IPSC charge (pC)
2.5
2.0
1.5
1.0
0.5
MTR
young

Figure S4

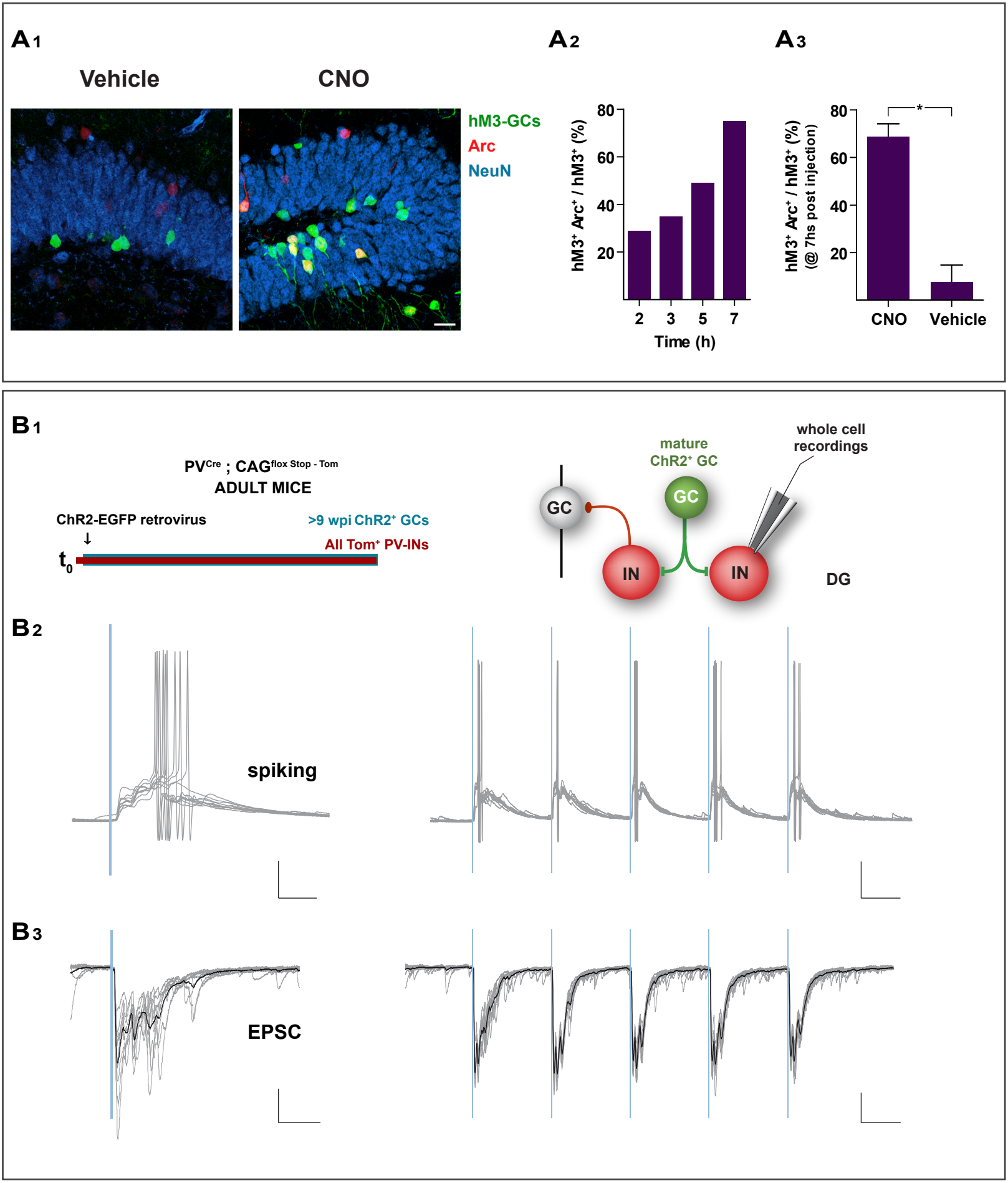
A1
Vehicle
CNO
hM3-GCs
Arc
NeuN
A2
hM3+ Arc+ / hM3+ (%)
80
60
40
20
2
3
5
7
Time (h)
A3
hM3+ Arc+ / hM3+ (%)
(@ 7hs post injection)
80
60
40
20
*
CNO
Vehicle
B1
PVCre ; CAGflox Stop - Tom
ADULT MICE
ChR2-EGFP retrovirus
t0
>9 wpi ChR2+ GCs
All Tom+ PV-INs
mature
ChR2+ GC
whole cell
recordings
GC
GC
IN
IN
DG
B2
spiking
B3
EPSC

Figure S5

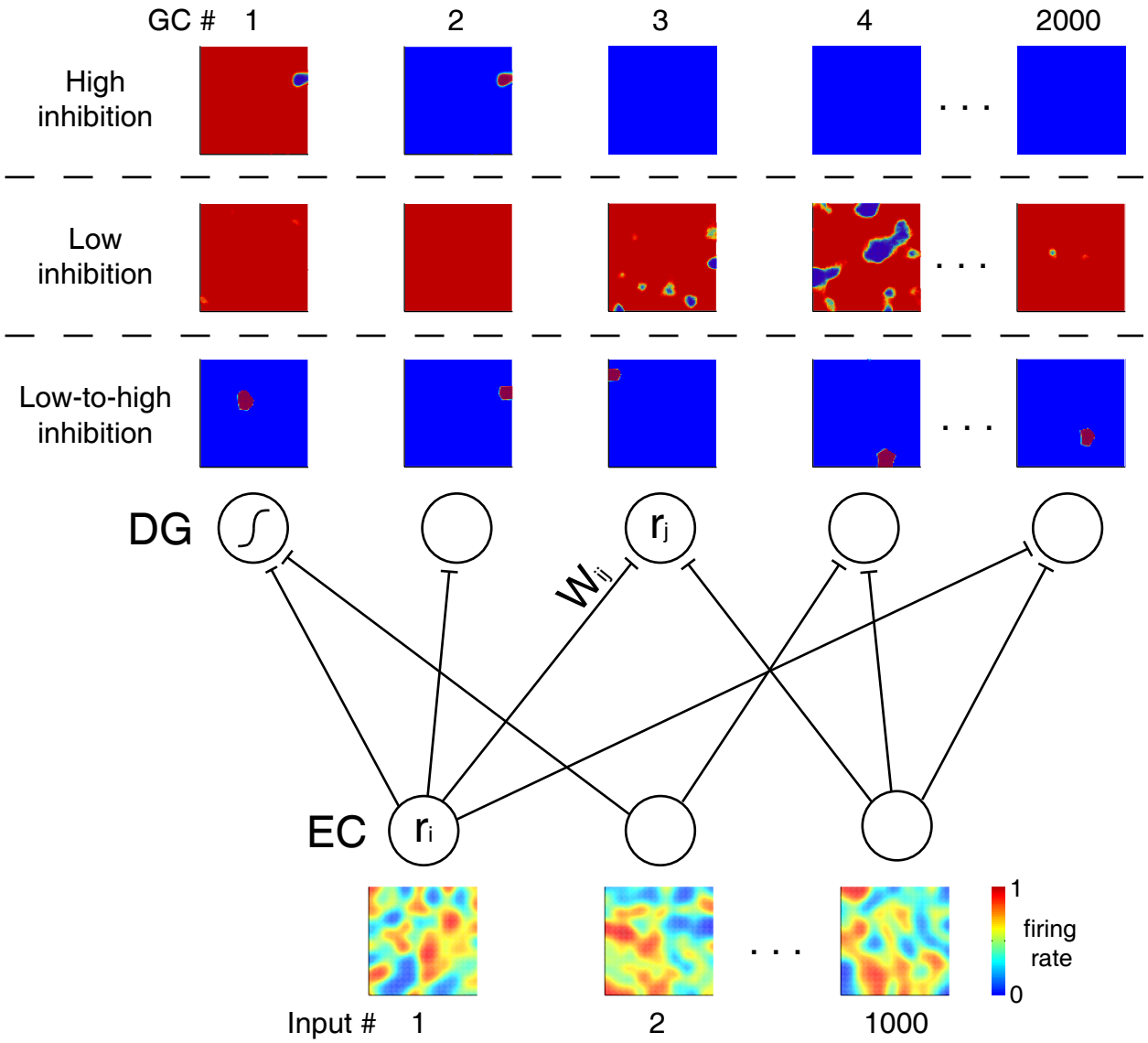
GC # 1
2
3
4
2000
High inhibition
Low inhibition
Low-to-high inhibition
DG
EC
r_j
W_{ij}
r_i
1
firing rate
0
Input # 1
2
1000

Figure S6

SUPPLEMENTAL FIGURE LEGENDS

Figure S1A. Schematic describing the experimental timelines utilized to monitor functional output of different GC populations. Colored arrows indicate the labeling times for GCs generated during postnatal development (purple) or adulthood (blue). Horizontal arrows denote the timing of functional assays. Three major populations of principal neurons were studied: mature GCs generated during early postnatal development (born at P11), mature GCs generated during adulthood (born at 6 weeks of age), and newly generated immature GCs (born at 6 weeks of age).

Figure S1B, related to Figure 1. Characterization of mature GCs generated during development in Ascl1^{CreERT2};CAG^{floxStopChR2} mice. (B1) Single confocal plane (1-µm thick) of hippocampal section depicting 9-week-old GCs expressing ChR2-EGFP (green) generated at P11. The red and blue channels display immunofluorescence for the immature GC marker DCX and the mature GC marker Cb. Note that most ChR2-GCs express Cb (79.8 %, N = 178 ChR2-GCs), with only a minor fraction expressing DCX (7.1%), supporting the notion that the majority of ChR2-GCs are mature. Scale bar: 20 µm. (B2) Visualization of dendritic spines in ChR2-GCs by confocal reconstruction from 23 optical sections 1-µm thick. Scale bar: 2 µm.

Figure S2, related to Figure 2. (A) Detailed analysis of postsynaptic responses evoked by optogenetic stimulation of young and mature ChR2-GCs generated in the adult hippocampus. (A1) Spiking latency in response to the 1-ms laser pulse is shown for young and mature ChR2-GCs, $p = 0.91$, with N = 6 (young) and N = 10 (mature). (A2) Profile of laser-evoked IPSCs on GCs. Peak IPSC amplitude: (***) denotes $p < 0.001$, N = 26 (young) and 41 (mature). IPSC success probability: (***) denotes $p < 10^{-4}$, N = 26 (young) and 41 (mature). IPSC rise time: $p = 0.52$, N = 14 (young) and 38 (mature). Latency to IPSC onset: (*) $p < 0.05$, N = 14 (young) and 40 (mature). (A3) Electrophysiological profile of laser-evoked EPSCs on CA3 pyramidal cells. Peak EPSC amplitude: $p = 0.89$, N = 12 (young) and 13 (mature). EPSC success probability: $p = 0.28$, N = 12 (young) and 13 (mature). EPSC rise time: $p = 0.11$, N = 9 (young) and 8 (mature). Latency to EPSC onset: $p = 0.74$, N = 9 (young) and 8 (mature). (A4) Electrophysiological profile of laser-evoked IPSCs on CA3 pyramidal cells. Peak IPSC amplitude and IPSC success probability; (*) and (**) denote $p < 0.05$ and $p < 0.01$, N = 13 (young) and 16 (mature). IPSC rise time: $p = 0.96$, N = 11 (young) and 15 (mature). Latency to IPSC onset: $p = 0.64$, N = 11 (young) and 15 (mature). (A5) Comparison of onset latencies of EPSC and IPSC (combined young and mature) recorded from pyramidal neurons: $p = 0.14$, N = 17 (EPSCs) and 26 (IPSCs). Statistical analysis was performed by two-tailed Mann-Whitney's tests. PSC success probability depicts the proportion of postsynaptic responses without failure.

(B) Short-term plasticity of FBI in response to trains. (B1) Experimental design and local DG network activated by trains of 5 laser pulses (1 ms, 10 Hz). (B2) Light trains delivered to young and mature ChR2-

GCs elicit multiple IPSCs recorded at 0 mV in unlabeled GCs. Traces depict all sweeps in the experiment (gray) and their average (black). Scales: 50 pA, 100 ms. (B3) IPSC charge for the individual pulses of the train delivered to young and mature GCs recorded in unlabeled mature GCs. (B4) Total inhibitory charge (integrated during 500 ms; with N = 12 young and N = 22 mature). (*) corresponds to $p < 0.02$ after Mann-Whitney's test. (***) and (**) denote $p < 0.001$ and $p < 0.01$ after ANOVA followed by post-hoc Bonferroni's test.

All data are depicted as mean ± SEM.

Figure S3, related to Figure 3. Optogenetic activation of mature GCs paired to mPP stimulation enhances the inhibitory synaptic current onto mature GCs. (A) Experimental design. A ChR2-EGFP retrovirus was injected in the adult DG and acute slices were obtained 4 (orange) or 7 (blue) weeks later. (B) Simplified diagram of the recording configuration. A stimulation electrode (stim) was placed on the medial perforant path (mPP) and whole-cell recordings were conducted on unlabeled mature GCs. Cell attached recordings were performed to measure spiking in response to mPP stimulation at the onset of the experiment. (C-D) Representative experiments for assessing the effect of optogenetic stimulation of young (C) or mature (D) ChR2-GCs on IPSCs elicited by mPP stimulation. IPSCs were measured while holding the membrane at 0 mV, with combinations of different stimuli: i) laser-mediated activation (blue line, 2 ms) of ChR2-GCs alone to recruit FBI (light); ii) mPP stimulation alone (artifact) to recruit FFI (PP)(Marin-Burgin et al., 2012); iii) mPP paired with laser (PP + light, paired at -10 ms); iv) mPP alone to re-assess the baseline (PP post). EPSCs were monitored at -70 mV after mPP stimulation to define the integration interval of IPSC values (shaded box), measured from onset to peak of the EPSC (C1, D1). Expanded views of IPSCs are shown (C2, D2). The peak amplitude of FBI current evoked by optogenetic stimulation (light) was much smaller than FFI current after mPP activation (PP), yet it was sufficient to significantly enhance the inhibitory charge during the phase of signal integration when both loops are recruited (PP+light). This is due to the fact that the FBI current reaches its peak at a time when the FFI is beginning to rise. Scales: 200 pA, 10 ms (C1, D1); 100 pA, 2 ms (C2, D2). (E) Synaptic charge of laser-evoked IPSCs is larger for mature than young ChR2-GCs (similar to data shown in Fig. 2J). Hollow symbols correspond to the example traces. (F) Optogenetic preactivation of ChR2-GCs enhances the inhibitory synaptic charge onto mature GCs. For quantitation, the IPSC charge was integrated from onset to peak of the EPSC, just before spiking, and the normalized difference between mPP stimulation alone and mPP paired with light is presented. Synaptic charge was enhanced in both groups by optogenetic pairing, with a significantly larger increment for mature vs. young ChR2-GCs. Data were obtained from 10 cells/3 mice (young) and 12 cells/5 mice (mature). (**) denote $p < 0.01$, two-tailed Mann Whitney's test. All data are depicted as mean ± SEM.

Figure S4, related to Figure 4. (A) Tom-labeled GCs obtained from GLAST^{CreERT2};CAG^{floxStopTom} mice display typical properties of 4 wpi GCs. (A1) Single confocal plane of dentate gyrus from GLAST^{CreERT2};CAG^{floxStopTom} mice four weeks after TAM administration (50 µg/g/day for 2 days). Four-week-old Tomato^{+} GCs are shown in red, combined with immunofluorescence for either Cb (left) or DCX (right), both shown in blue. Scale bar: 20 µm. (A2) Cb and DCX expression by young Tom-GCs. N = 3 mice (Cb) and N = 4 mice (DCX). (A3-4) Electrophysiological characterization of intrinsic properties of young Tom-GCs. (A3) Representative traces of whole-cell current clamp recordings. *Left*: Spiking elicited by depolarizing current steps of increasing amplitude as indicated at the left of each trace. Scales: 150 mV, 200 ms. *Right*: A magnified single spike where afterhyperpolarization (a property of mature spikes) can be clearly seen. Scales: 25 mV, 5 ms. (A4) Distribution of data recorded in voltage clamp corresponding from left to right to: number of spikes for maximal current steps (130 pA, 500 ms),membrane capacitance, resting membrane potential, and membrane input resistance, for N = 15 GCs. The properties measured in young Tom-GCs are very similar to those observed in retrovirally labeled GCs at 4 wpi (Mongiat et al., 2009).

(B) Detailed analysis of postsynaptic responses evoked by optogenetic stimulation of mature ChR2-GCs onto young (Tom-GCs) and mature (unlabeled) GCs in GLAST^{CreERT2};CAG^{floxStopTom} mice. (B1-4) Electrophysiological profile of laser-evoked IPSCs onto young (Tom) and mature (MTR) GCs. (B1) Peak IPSC amplitude: $p < 0.001$, N = 28 (young) and 25 (mature). (B2) IPSC success probability: $p < 0.05$, N = 28 (young) and 25 (mature). (B3) IPSC rise time: $p = 0.34$, N = 19 (young) and 23 (mature). (B4) Latency to IPSC onset: $p = 0.40$, N = 19 (young) and 24 (mature). (B5) Comparison of feedback inhibitory charge elicited by mature ChR2-GCs onto unlabeled mature GCs recorded from wild type (wt) and GLAST^{CreERT2};CAG^{floxStopTom} mice. As it may be noted, responses are very similar, with p = 0.39, and N = 32 (wt) and 25 (GLAST) mice. Statistical comparisons were performed by two-tailed Mann-Whitney's test. (B6) In all recordings Tom-GCs displayed substantial spontaneous excitatory activity. Example traces show a voltage-clamp recording with active spontaneous glutamatergic responses, typical for 4-week-old GCs. Scales: 5 pA, 500 ms (inset: 100 ms).

(C) Immature GCs elicit weak FBI onto both mature and immature GCs. (C1) *Upper panel*: Experimental design. GLAST^{CreERT2};CAG^{floxStopTom} mice received a ChR2-EGFP retrovirus in the right DG followed by administration of TAM. Mice were sacrificed 4 weeks later, rendering young GCs expressing either ChR2-EGFP or Tom (some GCs also displayed overlapping expression of both). *Lower panel:* Simplified network schematic depicting the recording conditions. Light stimulation of young ChR2-GCs activate local networks, and whole-cell recordings are obtained from young (Tom^{+}) or mature (unlabeled) GCs to compare the amount of FBI they receive. (C2) Peak amplitude (left) and synaptic charge (right) of laser-evoked responses, with N = 12 mature (MTR) and N = 15 young (Tom). No EPSC were observed (out of 25 recordings). All data are depicted as mean ± SEM.

Figure S5, related to Figure 5. (A) Characterization of the CNO-mediated activation of hM3Dq-expressing GCs. (A1) Confocal images of hippocampal sections containing 4 wpi hM3-GCs obtained 7 h after vehicle (left) or CNO (right) injection (5 µg/g, i.p.). Note that after CNO stimulation, hM3-GCs (green) increase the expression of the immediate early gene Arc (red). The GCL is labeled with NeuN (blue). Scale bar: 20 µm. (A2) Temporal course hM3-GC activation after CNO injection, expressed as percentage of GCs expressing Arc. (A3) CNO induces Arc expression in hM3-GCs after 7 h of CNO, but not vehicle. (*) denotes $p < 0.05$, with N = 5 mice (vehicle), N = 3 mice (CNO), two-tailed Mann-Whitney's test. Data are depicted as mean ± SEM.

(B) Spiking PV-INs evoked by stimulation of mature ChR2-GCs. (B1) Electrophysiological recordings of ChR2-GC → PV-IN synaptic connections in acute slices. Adult PV^{Cre};$CAG^{floxStopTom}$ mice received a ChR2-EGFP retrovirus in the DG and were sacrificed >9 weeks later, rendering mature GCs expressing ChR2-EGFP, and PV-INs expressing Tom (Tom-PV-INs). (B2) *Left*: Example whole-cell current clamp recording of a Tom-PV-IN showing action potentials in response to brief (1ms) light pulses (membrane potential was maintained at -70 mV; scales: 25 mV, 10 ms). *Right*: Train stimulation also elicited reliable spiking at 10 Hz (5 pulses, 1 ms; scales: 25 mV, 50 ms). (B3) Example whole-cell voltage clamp recording in the same Tom-PV-IN as in (B2) displaying EPSCs elicited by same stimuli as above. Scales: 200pA, 20ms (left panel); 200 pA, 50ms (right panel).

Figure S6, related to Figure 6. Architecture of the network model and examples of neural responses after learning with different inhibition protocols. The model network is built with 1000 input EC neurons and 2000 young DG neurons, with 50% connectivity. The activity of a neuron is represented by a firing rate between 0 and 1. For simplicity, a 2D surface is used as the novel input space, represented by a square of 100 x 100 pixels. Example responses of EC neurons for each point in the input space are shown in the bottom row. The strongest responses of DG neurons after learning are shown in the top rows, each row corresponding to a different inhibition protocol (from top to bottom: low inhibition, high inhibition and low-to-high inhibition). When learning occurs under conditions of low inhibition conditions, 214 neurons develop strong responses, but exhibit in general very wide and overlapping fields. Under high inhibition, although initially many GCs strive for dominance, only 2 of them eventually develop a strong response, while the rest of the neurons remain silent. In the third case, when inhibition is initially low and is progressively increased, reaching high levels by the end of the training session, 92 neurons develop a strong response, specializing into small regions of the input space, with minimal overlap between their response fields.

SUPPLEMENTAL EXPERIMENTAL PROCEDURES

Genetically modified mice

Ascl1^{CreERT2} (*Ascl1$^{tm1(Cre/ERT2)Jejo}$/J)* mice (Kim et al., 2007) and CAG$^{floxStopChR2\text{-}EYFP}$(Ai32) (*Gt(ROSA)26Sor$^{tm32(CAG\text{-}COP4*H134R/EYFP)Hze}$*/J) mice (Madisen et al., 2012), both obtained from Jackson Laboratories, were crossed to generate Ascl1^{CreERT2};CAG^{floxStopChR2} mice. TAM induction (a single injection of 200 μg/g) was performed at postnatal day 11 (P11) to achieve expression of ChR2 in the progeny of Ascl1^{+} progenitors, then obtaining mature ChR2-GCs generated during early postnatal development.

GLAST^{CreERT2} mice (Mori et al., 2006), kindly provided by M. Götz, were crossed to CAG$^{floxStop\text{-}tdTomato}$ (Ai14) (B6;129S6-*Gt(ROSA)26Sor$^{tm14(CAG\text{-}tdTomato)Hze}$*/J) conditional reporter line (Madisen et al., 2010), obtained from Hongkui Zeng, to generate GLAST^{CreERT2};CAG^{FloxStopTom} mice. TAM administration (50 μg/g/day, two consecutive days) was carried out in adult mice to achieve indelible expression of td-Tomato (Tom) in adult-born GCs.

Pvalb$^{tm1(cre)Arbr}$ mice (Hippenmeyer et al., 2005), kindly provided by S. Arber, were crossed to CAG$^{floxStop\text{-}tdTomato}$ (Ai14) conditional reporter mice to generate PV^{Cre};CAG^{FloxStopTom} mice to label PV-expressing GABAergic interneurons (PV-Tom).

Slice preparation and electrophysiological recordings

Brains were removed into a chilled solution containing (mM): 110 choline-Cl^{-}, 2.5 KCl, 2.0 NaH2PO4, 25 NaHCO3, 0.5 CaCl2, 7 MgCl2, 20 dextrose, 1.3 Na^{+}-ascorbate, 0.6 Na^{+}-pyruvate, and 4 kynurenic acid (kyn). The right hippocampus was dissected and coronal slices (400 μm thick) were cut in a vibratome (Leica VT1200 S, Nussloch, Germany) and transferred to a chamber containing artificial cerebrospinal fluid (ACSF; mM): 125 NaCl, 2.5 KCl, 2 NaH2PO4, 25 NaHCO3, 2 CaCl2, 1.3 MgCl2, 1.3 Na^{+}-ascorbate, 3.1 Na^{+}-pyruvate, and 10 dextrose (315 mOsm). Slices were bubbled with 95% O2/5% CO2 and maintained at 30°C for >1 hour before experiments started. For experiments shown in Figure S4A, whole-cell recordings were performed using microelectrodes filled with (mM): 150 K-gluconate, 1 NaCl, 4 MgCl2, 0.1 EGTA, 10 HEPES, 4 ATP-tris, 0.3 GTP-tris, 10 phosphocreatine. A similar microelectrode solution without GTP was used for the experiments shown in Figure S5B.

Optogenetics. Whole-cell recordings were carried out in CA3 pyramidal cells or in GCs from slices containing several ChR2-GCs that were visualized by their EGFP or EYFP expression, as previously described (Toni et al., 2008). Light pulses (1 ms) were delivered at 0.07 Hz while postsynaptic currents were recorded in voltage-clamp. EPSCs were isolated by voltage clamping the neurons at the reversal potential of the IPSC (Vh = -70 mV), whereas IPSCs were recorded at the reversal potential of the EPSC (Vh = 0mV). Glutamatergic currents were blocked by KYN 6 mM or NBQX 20 μM, and GABAergic currents were blocked by PTX 100 μM.

FBI onto immature GCs Adult GLAST^{CreERT2};CAG^{FloxStopTom} mice were used. A cohort of adult-born neurons was retrovirally transduced to express ChR2-GFP, as described above. Three to 4 weeks later the same

animals received intraperitoneal administration of TAM to induce Tom in new GCs. Mice were sacrificed 4 weeks later and acute slices containing 7 or 8-week-old ChR2-GCs (mature) and 4-week-old Tom-GCs were prepared. Whole-cell recordings were conducted on Tom-GCs and laser-evoked postsynaptic currents were measured. FBI was compared to that of unlabeled mature GCs located on the outer third of the GCL (Marin-Burgin et al., 2012).

Analysis of electrophysiological recordings

Statistical methods were used to differentiate light-responsive cells and light-evoked events from spontaneous activity using in-house Matlab routines. Events were identified as peaks in the low-pass filtered current (<250 Hz) when exceeded 4 standard deviations of the noise level (measured at >500 Hz high-pass filtered current). The onset of an event was defined as the time in which 20 % of the maximum amplitude was reached in the unfiltered signal. Once all events were identified, a cell was classified as responsive to light stimulation if there was a tendency greater than chance for events to accumulate around a given onset no longer than 30 ms (GCs and interneurons) or 50 ms (pyramidal cells) after light stimulation ($p < 0.05$). In order to achieve such a classification, the probability distribution of a similar accumulation of spontaneous events happening by pure chance was determined for each cell using a 2000-step shuffling procedure. Once a cell was classified as responsive to light, spontaneous and light-evoked events were differentiated. Since light-evoked events formed a tight peak distribution, events further away than 2.5 standard deviations around the median onset with respect to the stimulus were classified as spontaneous and discarded in recursive steps, until no events stood out of bounds. The charge of light-evoked events was measured within a 20 ms time window starting at the onset of the event.

In vivo assays

Mice were anesthetized and CAG-hM3Dq-2A-EGFP retrovirus (1.5 µl) was infused into right dentate gyrus as described above. Control mice were injected with a retrovirus encoding for CAG-EGFP. Four (4) or 8 weeks after retroviral injection mice were prepared for exposure to enriched environment. Enriched environment was utilized to generate a basal level of neuronal activity in both hippocampi, ipsilateral and contralateral to the retroviral injection. Mice received a single intraperitoneal CNO injection (5 µg/g), and 90 min later they were placed in an enriched environment for 30 min in groups of 4 animals (hM3) or 2 animals (control, GFP). Mice were then returned to their cages for 30 min, were then anesthetized, and perfused with 4 % paraformaldehyde. Coronal sections (40-µm thick) were prepared for immunofluorescence analysis to count the number of active HM3-GCs (by Arc expression) and parvalbumin GABA interneurons (by c-Fos expression). To obtain accurate comparisons, counts for the different markers were done in sections obtained from the same mice, and paired analysis was performed by comparing the right hemisphere ipsilateral to the presence HM3-GCs vs. left hemisphere, contralateral to the injected side. Experiments involved 4 – 5 mice / experimental condition, and cell counts were performed in 1 every

12 sections (40-μm thick) obtained from the septal region (bregma -1.06 to -2.18). All sections analyzed within this interval displayed retrovirally-labeled GCs.

Immunofluorescence

Immunostaining was done on 40-μm or 60-μm free floating coronal sections throughout the fixed brain, analyzing up to 3 sections to obtain ≥ 20 GFP cells to each dentate gyrus per mouse. Antibodies were applied in TBS with 3% donkey serum and 0.25% Triton X-100. Double or triple labeling immunofluorescence were carried out using the following primary antibodies: Arc (rabbit polyclonal 1:500, Synaptic Systems), c-Fos (Calbiochem 1:20000), calbindin D-28k (rabbit polyclonal 1:1000, Swant), DCX (rabbit polyclonal 1:750, a gift from C. Walsh), GFP (rabbit polyclonal 1:100, Invitrogen; or chicken polyclonal 1:500, Millipore; or chicken polyclonal 1:500, AVES), NeuN (mouse monoclonal 1:50; a gift from F. H. Gage), parvalbumin (mouse monoclonal !:1000, Swant), and RFP (rabbit polyclonal 1:200, Chemicon). For Cb immunolabeling, pre-incubation with methanol (15 min) was included to enhance penetrability. Corresponding secondary antibodies were used: donkey anti-mouse Cy5, donkey anti-rabbit Cy3 or donkey anti chicken Cy2, 1:250 (Jackson ImmunoResearch, West Grove, PA).

Confocal microscopy

Images were acquired using a Zeiss LSM 5 Pascal or a Zeiss LSM 710 NLO confocal microscopes (Zeiss, Jena, Germany). Colocalization of fluorescent markers was assessed in three-dimensional reconstructions through Z-stacks using multiple planes for each cell. Images were taken at 1-μm intervals using an optical slice of 0.7-1 μm corresponding to an airy unit of 1 for each fluorophore (40x oil immersion objective, NA 1.4).

Computational model

The model was built with 1000 input entorhinal cortex (EC) neurons projecting to 2000 young GCs. The activity of a neuron at a given time is represented by a firing rate r, set to be for simplicity between 0 (silent) and 1 (active). Connections between EC and DG neurons were established at random with a probability of 0.5. If a connection between EC neuron i and DG neuron j existed, its synaptic weight W_{ij} was initially set to be a random number between 0 and 1. The novel input space (Fig. 6) that constituted the training set of patterns was set to be a 2D square for graphical convenience. It was divided into 100 x 100 pixels and for each pixel a random response was assigned to each EC neuron. The collection of all responses for a given EC neuron was then smoothed with a 10 pixel-wide Gaussian filter, in order to obtain slow varying inputs (Figure S6). At every learning step, a point was chosen at random inside the 2D square, which defined the corresponding activity r_i for each EC neuron. This activity was propagated to the DG layer using the matrix of synaptic weights W_{ij}, such that a GC j was subject to an input field

$$h_j = \sum_i W_{ij} r_i,$$

where the sum is performed over all afferent connections. The firing rate of neuron j was then obtained by applying a sigmoid function to the input field

$$r_j = \left[1 + \exp(-(50 * (h_j - I))\right]^{-1},$$

where r_j is the firing rate of GC j and I is the inhibition controlling the overall activity of the network. The inhibition was set to be the k^{th} percentile of the h_j distribution, and different values of k defined 3 different learning strategies. A low value of this parameter ($k = 90$) defined the low inhibition protocol and a high value ($k = 99.5$) defined the high inhibition protocol. The third protocol, low-to-high, used an initially low value ($k \sim 90$) that increased slowly, reaching a high level ($k \sim 99.5$) by the end of the training session. Such a protocol mimics the progressive insertion of young DG cells into the inhibitory network. In this way, at step n of the training session, the inhibition for the low-to-high protocol was defined by

$$k = 90 + 9.5 * \left[1 - \exp\left(-{}^{n}/_{250}\right)\right].$$

Note that the value of k for high inhibition was chosen to ensure that only one neuron at a time could be active, simplifying the graphical interpretation (Fig. 6). However, allowing for more neurons to be active simultaneously does not alter qualitatively the results. Note also that the value of k was the only difference between protocols, which, for the rest, were run under identical conditions (initial values, training set, learning rules).

Once the activity r_i of all EC neurons and r_j of all GCs were determined, the synaptic weights were modified through the hebbian incremental rule

$$W_{ij} = W_{ij} + 0.002 * r_i * r_j,$$

favoring the potentiation of synapses where both pre- and post-synaptic neurons were highly active. This strictly incremental rule causes an unbounded increase of all synaptic weights. To prevent this, the vector of all incoming weights to each neuron j was normalized at each learning step by its Euclidean norm $\sqrt{\sum_i {W_{ij}}^2}$. Following this, a new input was chosen and the learning process went on until all elements in the training set were used. The training set was large enough to ensure that by the end of the training session all protocols would have reached stability (Fig. 6D).

Analysis of pattern separation and convergence

After training the network with some of the 3 inhibition protocols, 50000 pairs of points belonging to the novel input space were chosen at random. Each point of the pair defined a population vector of input activity (EC layer) and a population vector of output activity (DG layer). The correlation of pairs of output

vectors was plotted against the correlation of pairs of input vectors (Fig. 6E). When outputs are more similar than inputs, representations are converging, while the opposite case characterizes pattern separation. Cells that were silent across all novel inputs were left out of the analysis.